FRETTING FATIGUE LIFE PREDICTION USING THE EXTENDED FINITE ELEMENT METHOD

C. Navarro[1], E. Giner[*,2], M. Sabsabi[2], M. Tur[2], J. Domínguez[1], F.J. Fuenmayor[2]

[1]Departamento de Ingeniería Mecánica y de los Materiales, E.T.S. de Ingenieros,
Universidad de Sevilla, Camino de los Descubrimientos, 41092 Sevilla, España.
E-mail: cnp@us.es
Tel: +34 954481365

[2]Departamento de Ingeniería Mecánica y de Materiales-CITV, E.T.S. de Ingenieros Industriales,
Universidad Politécnica de Valencia, Camino de Vera s/n, 46022 Valencia, España.
E-mail: eginerm@mcm.upv.es
Tel: +34 963877007 Ext. 76218.

ABSTRACT

In this work, fretting fatigue tests available in the literature are modeled using the extended finite element method (X-FEM). The aim is to numerically evaluate the stress intensity factors (SIFs) for cracks of different lengths emanating at the end of the contact zone and to estimate the propagation life corresponding to each of the tests. This propagation life is combined with the initiation life calculated analytically using a multiaxial fatigue criterion (Fatemi-Socie), following a initiation-propagation approach for life estimation. The predicted lives are then compared with the reported experimental lives. It is shown that the consideration of the crack-contact interaction through the numerical models tends to improve the life estimation when compared with a fully analytical approach for the calculation of both initiation and propagation lives.

KEYWORDS: Fretting-fatigue. Extended finite element method (X-FEM). Initiation and propagation life model.

1 INTRODUCTION

In the analysis of the fretting fatigue life and other fatigue problems, two stages are usually distinguished: initiation of the crack and its subsequent propagation. In recent years, methods have been proposed to predict the total life as a combination of the life spent during the initiation phase and the life associated with the propagation phase. The point at which the initiation phase finishes and the propagation phase begins cannot be precisely defined and some authors propose a certain transition crack length on a rather heuristic basis. In this work, we use a variable initiation length model proposed in [1, 2], in which the transition length is not previously fixed, but it depends on the particular load conditions and material properties of the analyzed problem.

The initiation life can be estimated by means of multiaxial fatigue criteria, such as the McDiarmid and the Fatemi-Socie criteria, which are reported to give good results [2]. The propagation life can be analyzed using a crack growth law of the type $\mathrm{d}a/\mathrm{d}N = f(\Delta K)$, e.g. Paris law or other variations based on linear elastic fracture mechanics assumptions (LEFM). The correct calculation of the stress intensity factors (SIFs) plays a crucial role when predicting the life associated with the crack propagation stage. This can affect the estimated total life, especially for problems in which the propagation life is a significant part of the total life, for example in certain fretting problems in which the steep gradients in the vicinity of the contact induce a rapid crack initiation.

On the other hand, the propagation stage in a fretting-fatigue problem is substantially different from that of plain fatigue only during the phase in which the crack length is less than the characteristic dimension of the contact zone. Analytical approaches have been used [1] based on the weight function method for estimating the SIF. However, these methods do not take into account the influence of the crack-contact interaction (i.e. alteration of the contact fields due to the crack presence) which can be important at the beginning of the propagation stage.

For extracting realistic values of the SIFs including the crack-contact interaction, the numerical modelling of the problem becomes necessary and the finite element method (FEM) or the more advanced extended finite element method (X-FEM) can be applied. To compute the propagation life, the SIFs must be calculated for a relatively wide range of crack lengths. This means that the mesh generation process needed in the classical FEM is very cumbersome, as it must conform to both relatively small contact zones and cracks of small size in their vicinity.

On the other hand, in recent years the X-FEM [3] has proved to be a very efficient tool for the numerical modelling of cracks in linear elastic fracture mechanics (LEFM). Compared to the standard FEM, the X-FEM presents great advantages for the numerical modelling of cracks. The main advantage is that it is not necessary to generate a mesh that conforms to the crack boundaries (faces) to account for the geometric discontinuity. Therefore only a single mesh, often generated easily, can be

used for any crack length and orientation, which enormously expedites the computation process. In addition, the method includes crack-tip enrichment functions that provide accurate estimations of the SIFs when using domain independent integrals, such as the J-integral or the interaction integral.

In this work, the use of the X-FEM is combined with the initiation-propagation model proposed in [1, 2] to assess the total life of fretting fatigue problems. The models analyzed correspond to 2D problems with cylindrical contact pressed onto flat specimens subjected to a variable bulk load. The predicted life is compared with the experimental results reported in the literature [4, 5] for fretting tests with cylindrical indenters and flat specimens. The propagation analyses have been performed by means of the X-FEM implementation carried out by the authors [6] in the framework of the commercial code ABAQUS. The results show that the use of the X-FEM to predict the propagation lives tends to improve the life estimation when compared to an analytical approach using weight functions.

2 COMBINED INITIATION-PROGAGATION MODEL

The model used to estimate life in fretting was proposed by the authors [1]. It is assumed that two different mechanisms act upon a material subjected to fretting: one during the initiation phase and another during propagation. The phenomena produced in either phase are considered different and are dealt with separately, although the consequence is the same: failure in the material.

Regarding the first phase, there is a calculation of the number of cycles needed to initiate a crack along the trajectory theoretically followed by it, N_i. This is done by evaluating the stresses along the assumed crack path and introducing them in the fatigue curve of the material. Due to the complexity of the stress field (multiaxial and non-proportional), a multiaxial fatigue criterion must be employed. In this case the well known Fatemi-Socie parameter is used.

In the second phase, the calculation is for the number of cycles needed to propagate the crack from each point until failure, using LEFM, N_p. This is done by integrating Paris crack growth law from each crack length to the final length, where the fracture of the specimen is assumed to occur. It will be assumed that the crack is initiated in the limit of the contact zone and grows perpendicular to the surface. It can be experimentally proven that these suppositions are not far from reality [1, 4].

The sum of the two curves obtained, N_i plus N_p, renders the total life associated to each point, considering each point as the crack length whose growth is governed first by initiation and then by propagation. The minimum of that curve is the most unfavourable point in it, which provides the life of the specimen. The position of the minimum, called initiation length, marks the end of the initiation and the beginning of propagation. This model supposes that before the initiation length the crack is initiated in each point before it has time to propagate. In contrast, once the initiation length is surpassed then propagation dominates over initiation and the evolution is predicted using fracture mechanics.

3 FUNDAMENTALS OF THE X-FEM

The essential feature of the method is the enrichment of the FE model with additional degrees of freedom (dof) for the nodes belonging to the elements geometrically intersected by the crack location (called enriched nodes and elements, respectively). Thus, the discontinuity is included in the numerical model without modifying the discretization. Fig. 1 shows a portion of the mesh used in this work, where the enriched nodes are marked. Nodes located next to the crack faces (encircled nodes in Fig. 1) are enriched with 2 additional dofs (one for each direction of the domain space) to represent the physical displacement discontinuity by means of a Heaviside function $H(\mathbf{x})$. The Heaviside function can only take the values $H(\mathbf{x}) = \pm 1$, depending on the relative position of the enriched node with respect to the crack faces.

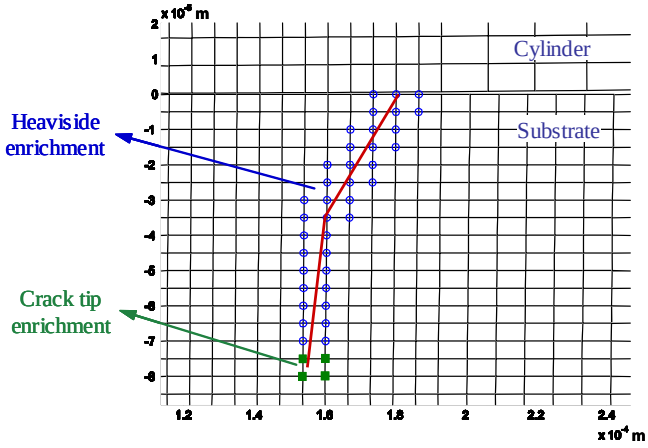

Figure 1: Enriched nodes in the X-FEM.

The X-FEM formulation allows for a further type of enrichment for those nodes that surround the crack-tip. These nodes (marked as squares in Fig. 1 are enriched with 8 additional dofs: four crack-tip functions $F_j(\mathbf{x})$ times the two directions of the domain space. The crack-tip functions constitute the basis functions that represent the first term of the LEFM displacement field, and consequently, reproduce the classical stress singular behavior of the LEFM. These functions are given by:

$$F_j(r,\theta) = \sqrt{r}\left[\sin\frac{\theta}{2},\ \cos\frac{\theta}{2},\ \sin\frac{\theta}{2}\sin\theta,\ \cos\frac{\theta}{2}\sin\theta\right] \quad (1)$$

with $j = 1-4$. Thus, for the 2D case, the extended finite element approximation to the displacements at a point of the domain $\mathbf{x}$ is:

$$\mathbf{u}_{\mathrm{xfem}}(\mathbf{x}) = \sum_{i=1}^{nn_{\mathrm{M}}} N_i(\mathbf{x})\mathbf{u}_i + \sum_{i=1}^{nn_{\mathrm{H}}} N_i(\mathbf{x})H(\mathbf{x})\mathbf{a}_i + \\ + \sum_{i=1}^{nn_{\mathrm{CT}}} N_i(\mathbf{x}) \left(\sum_{j=1}^{4} F_j(\mathbf{x})\mathbf{b}_{i,j} \right) \quad (2)$$

where nn_{M} is the number of nodes in the mesh, and nn_{H}, nn_{CT} are the number of Heaviside and crack-tip nodes, respectively. $N_i(\mathbf{x})$, $\mathbf{u}_i$ are the standard shape functions and dof of each node i, respectively, and $\mathbf{a}_i$, $\mathbf{b}_{i,j}$ are the additional dof associated with the Heaviside function $H(\mathbf{x})$ and the crack-tip functions $F_j(\mathbf{x})$. Note that the introduction of the crack-tip functions enhance the quality of the calculated singular LEFM fields in the vicinity of the crack-tip, yielding more accurate estimations of the SIFs. This is a further advantage of the X-FEM over the standard FEM [3].

The authors have implemented the X-FEM approach in ABAQUS by defining a user element that allows 12 dof/node [6]. The combination of the powerful contact procedures available in ABAQUS with the X-FEM implementation has proved successful, as shown in the next sections. The SIFs calculation has been done by means of the path-independent interaction integral [7]. The interaction integral features the same advantages as the J-integral for the SIF computation, like good accuracy and little user intervention. In addition enables the extraction of K_{I} and K_{II} for mixed-mode problems by using auxiliary fields. When the interaction integral is recast as an equivalent domain integral, it has the following form:

$$I^{(1,2)} = \int_{\Omega} \left[\sigma_{ij}^{(1)} \frac{\partial u_i^{(2)}}{\partial x_1} + \sigma_{ij}^{(2)} \frac{\partial u_i^{(1)}}{\partial x_1} - W^{(1,2)}\delta_{1j} \right] \frac{\partial q}{\partial x_j} \mathrm{d}\Omega \quad (3)$$

where $^{(1)}$ are the actual fields of the problem approximated by the X-FEM solution and $^{(2)}$ are the auxiliary fields. These fields are chosen to be the asymptotic crack-tip fields for pure mode I or pure mode II to compute K_{I} and K_{II} respectively. In (3), x_1, x_2 are the local directions with respect to the crack-tip, δ_{1j} is the Kronecker's delta and q is an arbitrary and continuous function which must vanish at the outer boundary of the problem domain and take the value 1 at the crack-tip. The SIFs of the problem are then calculated as follows:

$$K_{\mathrm{I}} = \frac{E'}{2} I^{(1,\mathrm{aux\ mode\ I})} \quad ; \quad K_{\mathrm{II}} = \frac{E'}{2} I^{(1,\mathrm{aux\ mode\ II})} \quad (4)$$

where $E' = E$ for plane stress and $E' = E/(1-\nu^2)$ for plane strain. The q-function used in this work is an annular function defined by a radius r_q measured from the crack-tip, in the same fashion as in [3]. Note that the application of the interaction integral to the X-FEM results must include the contribution of both standard elements and enriched elements where $\frac{\partial q}{\partial x_j} \neq 0$.

4 APPLICATION TO FRETTING-FATIGUE TESTS

4.1 Experimental tests used for comparison

Fig. 2 shows a sketch of the fretting fatigue tests modelled in this work. The test rig consists of two cylindrical fretting pads contacting onto the flat surface of a specimen made of the same material. The normal load P is held constant during the test originating a contact region of semi-width a. A variable bulk stress σ_{B} is applied to the specimen. Due to the coefficient of friction f, a tangential load Q is generated on the fretting pad. The values of the tangential load and the bulk stress on the left part of the specimen depend on the compliances of both the specimen and the fretting pad support (in Fig. 2 A_{s} denotes the cross-sectional area of the specimen). Under the loading conditions analyzed in this study, it is well known [8] that the contact area is divided into an internal stick zone of semi-width c and two slip zones. The stick zone has an eccentricity e measured from the center of the contact zone (see Fig. 2).

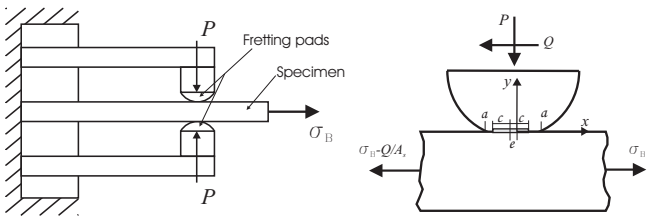

Figure 2: Sketch of the fretting fatigue tests with cylindrical pads and loads transmitted.

Two sets of fretting fatigue tests are analyzed in this paper. The first one, referred here as S&F [4], uses the material Al2024 T351. Not all the tests found in [4] are studied in this paper, only a sample including the whole range of lives. In these tests the specimens thickness was 12.7 mm and the friction coefficient 0.65. Different radii were used for the cylinders, varying between 127 and 229 mm. The test conditions are summarized in Table 1.

The second set of tests analyzed, referred here as A&N [5], was performed with the aluminium alloy Al4%Cu, which is very similar to the preceding one. As in the previous group, only a sample including the whole range of lives is studied. The specimens thickness was 12.5 mm and the friction coefficient 0.75. In these tests the radii of the contact pads were between 50 mm and 150 mm (see Table 2). The Young's modulus and Poisson's ratio is the same for both materials, 74.1 GPa and 0.33, respectively. Finally, other parameters needed for the calculations are

shown in Table 3. The crack growth properties are given for a stress ratio of $R = 0$ and cycles/meter, MPa$\sqrt{\text{m}}$.

Table 1: Tests and lives reported by S&F in [4]

Test	P (kN)	Radius R (mm)	σ_{Bulk} (MPa)	Q/P	N_{failure} (cycles)
1 (MAF1a)	5.454	229	111.7	0.43	238000
2 (MAF4x)	5.370	127	88.4	0.35	563946
3 (MAF5a)	7.226	127	101.9	0.31	545489
4 (MAF9x)	6.268	229	85.4	0.32	856524
5 (MAF14x)	5.293	229	81.0	0.31	867330
6 (MAF15x)	5.325	229	82.9	0.26	768364
7 (MAF21x)	7.153	229	97.9	0.24	463324
8 (MAF22x)	6.176	178	84.7	0.27	621442

Table 2: Tests and lives reported by A&N in [5]

Test	p_0 (MPa)	Radius R (mm)	σ_{Bulk} (MPa)	Q/P	N_{failure} (cycles)
1	157	50	92.7	0.45	1290000
2	157	75	92.7	0.45	670000
3	143	100	92.7	0.45	610000
4	143	50	77.2	0.45	1200000
5	143	100	77.2	0.45	610000
6	120	150	61.8	0.45	1230000

Table 3: Properties of alloys Al2024 T351 and Al4%Cu.

Material		Al2024 T351 [4]	Al4%Cu [5]
Tensile strength	σ_u	470 MPa	500 MPa
Yield strength	σ_y	310 MPa	465 MPa
Fatigue limit	σ_f	230 MPa	206 MPa
Fatigue strength coefficient	σ_f'	714 MPa	1015 MPa
Fatigue strength exponent	b	-0.078	-0.11
Paris law coefficient	C	$6.529 \cdot 10^{-11}$	$1.74 \cdot 10^{-10}$
Paris law exponent	n	3.387	4

4.2 Description of the numerical models

A 2D finite element model of the fretting fatigue tests has been defined, as depicted in Fig. 3. The rectangle $2L \times h$ corresponds to the specimen and has a length of $2L = 40$ mm. The half thickness h and the pad radius R is varied according to the test, as well as the friction coefficient f considering a Coulomb's friction model. The crack modelled with X-FEM is located at the right end of the contact zone included in the specimen at $x = a$. Note that the crack length is denoted as a_c. Vertical displacements are constrained on the bottom line of the specimen. Further restrictions for displacements are applied at nodes located on the shaded sides shown in Fig. 3. Using multipoint constraints (MPCs) the displacements in the x-direction of all nodes located at $x = -L$ and $x = L$ are forced to be identical. Similarly, displacements at nodes on the pad top are enforced to be equal. The application of the force T produces a bulk stress and the amount of the tangential force Q transmitted through the frictional contact is controlled by the relative stiffness of the equivalent springs. The equivalent compliances of the left portion of the specimen and the pad support are replaced by spring elements with stiffness k_s and k_p respectively, as shown in Fig. 3. The spring stiffnesses have been varied in order to set the different ratios Q/fP for each test.

The solution is obtained in two steps. First, the normal load P is applied. Rigid body motion of the specimen is avoided by imposing a restriction in the x-direction of nodes at $x = -L$ and $x = L$. In a second step this restriction is eliminated and a monotonically increasing load T that generates the bulk stress σ_{B} is applied. Since the contact problem is non-linear, loads must be applied in small time increments in order to obtain the correct stress distribution.

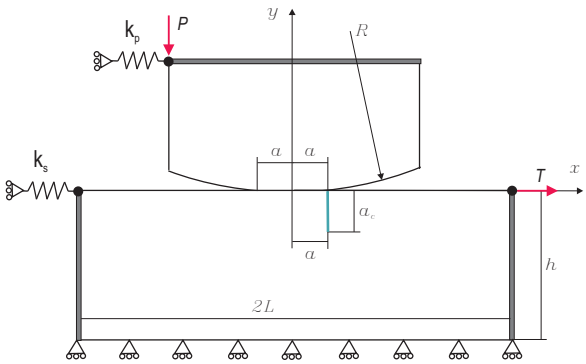

Figure 3: Geometry of the numerical model.

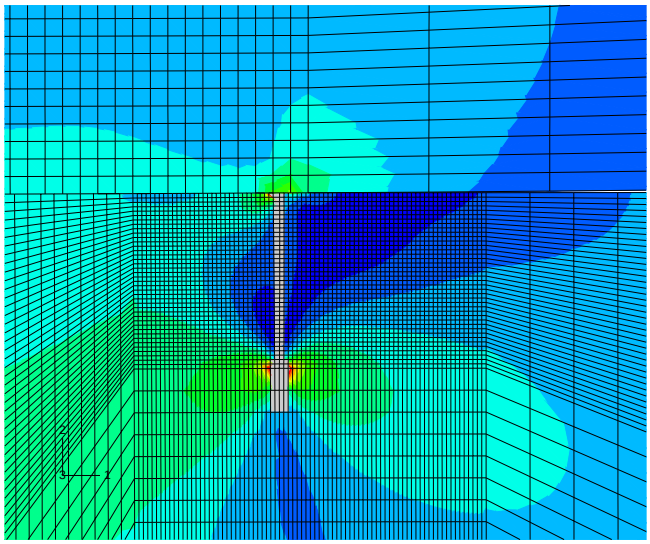

Figure 4: Von Mises contour plot for the test 1 of the A&N series for a crack length of $100\ \mu\text{m}$*. Elements in grey are the X-FEM enriched elements.*

Fig. 4 shows an example of one of the analyses carried out for a crack length of $100\ \mu\text{m}$ at the end of the contact zone with the implementation of X-FEM in ABAQUS. The location $x = a$ is estimated for each of the tests by solving the corresponding FE problem (without a crack) and verifying that the value is in good agreement with the analytical estimation for the cylindrical contact on a half-plane. In Fig. 4, it can be observed that the stress distribution is both affected by the contact and the crack

presence. A detailed analysis of the crack-contact interaction is given in [9]. In order to determine the SIF K_{I} as a function of crack length a, a series of lengths a has been analyzed for each test without modifying the underlying mesh thanks to the versatility of the X-FEM method. The results are discussed in the following section.

4.3 SIF calculation

Fig. 5 shows the values of the SIFs K_{I} obtained with X-FEM and the Eq. (4). These results are compared to the analytical estimation using the weight function method [10]. In the weight function method (WF), the stress distribution along the crack location (solved for a configuration with no-crack) is combined with a WF w derived for a given geometry to yield K:

$$K_{\mathrm{I}}^{\mathrm{WF}} = \sqrt{\frac{2}{\pi}} \int_0^{a_{\mathrm{c}}} \sigma_x(x,y) w(y)\, \mathrm{d}y \qquad (5)$$

For the case of a straight crack normal to the surface at the end of the contact zone, the analytical stresses σ_x are evaluated at $x = a$. These stresses must include the contribution of the normal and shear contact loads plus the bulk stress. In this work we have used the WF w for a single-edge crack in tension (SENT) in a strip of finite width [10]. In Fig. 5, the WF estimations show differences with the X-FEM values, and can have an over- or underestimating trend. SIFs computed through X-FEM include the effect of crack-contact interaction and, therefore, are assumed to be more accurate. These differences have an influence on the predicted propagation life, as shown below.

As expected, for very short cracks, the agreement between the X-FEM and WF solutions is very good because the influence of the crack on the contact distribution is small. For longer cracks, the differences between both solutions are about 5%-10%. The cause of these differences is, in the first place, the consideration or not of crack-contact interactions. For much longer cracks, where this interaction is not noticeable, the cause of the difference is that the bulk stress is assumed uniform in the WF formulation. Indeed, this stress is not uniform in the vicinity of the contact, since the axial forces in the specimen are not the same on both sides of the contact (part of the axial load is diverted through the contact elements as shear load).

Another aspect that can be analyzed is the influence of the sticking zone offset e due to the bulk stress. In [9], it is verified that the eccentricity e tends to decrease as the crack length increases due to a "shadow" effect of the crack. Therefore, the shear stress distribution used in the analytical estimations of K_{I} should be corrected to account for this effect in a variable manner (depending on the crack length). Fig. 5 show the differences when K_{I} is computed through weight functions considering the full offset of the sticking zone, i.e. no crack effect ($e \neq 0$), and zero offset as for a sufficiently long crack ($e = 0$). As expected, the calculations with a full offset effect $e \neq 0$ are in good agreement with the X-FEM values only for very small cracks, whereas calculations with zero offset $e = 0$ tend to match the X-FEM values for longer cracks. Note that for longer cracks the dominant source of discrepancy is due to the non-uniform distribution of the bulk stress, as explained above. From this analysis it is clear that the variation of the eccentricity with crack length cannot be predicted *a priori* without considering the crack-contact interaction. Therefore the application of the weight function technique introduces simplifications that are overcome by the numerical methodology proposed here.

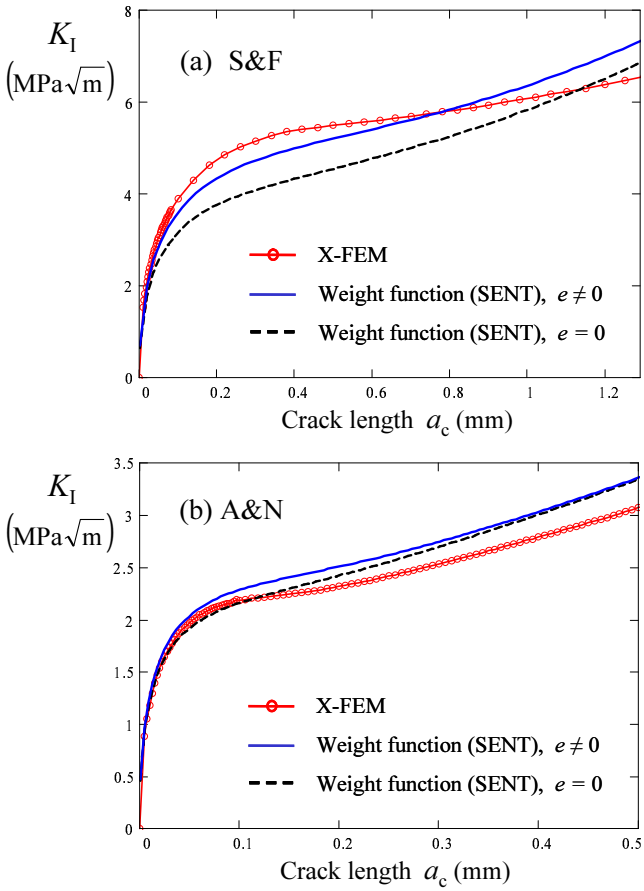

Figure 5: Values of K_{I} vs. crack length for (a) test 7 of the S&F series[4] and (b) test 4 of the A&N series [5].

4.4 Life prediction and correlation with experimental lives

Fig. 6 shows the predicted total life for each of the analyzed tests confronted to the experimental life reported in [4] and [5]. Two series of results are presented, in which the propagation life is calculated using the SIFs provided by X-FEM and by the WF method, respectively. The initiation life is practically the same in both cases and is calculated as given in Section 2. It can be observed

that the results given by the X-FEM tend to give slightly better results for most of the tests, which are closer to the experimental life. Although the estimated total life is similar for both approaches, the differences in the propagation life are about 20% (note the logarithmic scale of the plot). The fact that the initiation life can account for an important fraction of the total life in fretting tests with incomplete contacts does not lend itself to exhibit larger differences. Of course, there are many other factors that can affect the total real life that are not considered in the X-FEM or WF models.

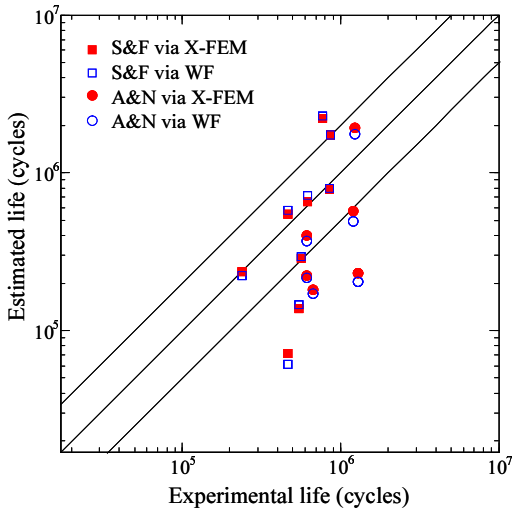

Figure 6: Correlation between the estimated and experimental lives.

It is interesting to observe that most results that are overestimated (underestimated) with the WF method are reduced (increased) with the X-FEM approach. Most of the S&F results tend to be overestimated with the WF method. However, X-FEM estimations tend to yield larger values of K_{I} than with WF as shown in Fig. 5(a), reducing the propagation life. For the A&N results, that tend to be underestimated, lower SIFs computations via X-FEM than with WF, Fig. 5(b), provide larger propagation lives.

5 CONCLUSIONS

In this work, propagation lives in fretting fatigue tests with cylindrical contacts are calculated numerically using an X-FEM approach. The advantage of using a numerical procedure is that the analyses incorporate the crack-contact interaction effects that cannot be included in analytical approaches, such as the weight function method. The use of the X-FEM makes this study feasible, because no remeshing is needed to study different crack lengths parametrically. This enables to compute the SIF as a function of crack length (an interaction integral is used for this purpose). The propagation lives are combined with an estimation of the initiation life following a variable-length initiation-propagation model. For a series of experimental tests reported in the literature, results show that the use of X-FEM to predict the propagation phase tends to improve the life estimation when compared to the weight function method.

ACKNOWLEDGEMENTS

The authors gratefully acknowledge the financial support given by the DGICYT of the Spanish Ministry of Science and Innovation (Projects DPI2007-66995-C03-01 and DPI2007-66995-C03-02).

REFERENCES

[1] Navarro C, García M, Domínguez J. A procedure for estimating the total life in fretting fatigue. *Fatigue Fract Engng Mater Struct* **26**, 459–468, 2003.

[2] Navarro C, Muñoz S, Domínguez J. On the use of multiaxial fatigue criteria for fretting fatigue life assessment. *Int J Fatigue* **30**, 32–44, 2008.

[3] Moës N, Dolbow J, Belytschko T. A finite element method for crack growth without remeshing. *Int J Numer Methods Engng* **46**, 131–150, 1999.

[4] Szolwinski MP, Farris TN. Observation, analysis and prediction of fretting fatigue in 2024-T351 aluminum alloy. *Wear* **221**, 24–36, 1998.

[5] Araújo JA, Nowell D. The effect of rapidly varying contact stress fields on fretting fatigue. *Int J Fatigue* **24**, 763–775, 2002.

[6] Giner E, Sukumar N, Tarancón JE, Fuenmayor FJ. An Abaqus implementation of the extended finite element method. *Engng Fracture Mech* **76**, 347–368, 2009.

[7] Chen FHK, Shield RT. Conservation laws in elasticity of the *J*-integral type. *J Appl Math Phys (ZAMP)* **28**:1–22, 1977.

[8] Hills DA, Nowell D. Mechanics of fretting fatigue. Kluwer Academic Publishers, Dordrecht, 1994.

[9] Giner E, Tur M, Vercher A, Fuenmayor FJ. Numerical modelling of crack-contact interaction in 2D incomplete fretting contacts using X-FEM. *Tribology Int* **42**, 1269–1275, 2009.

[10] Bueckner HF. Field singularities and related integral representations. In: Mechanics of Fracture 1. Methods of analysis and solutions of crack problems, ed. GC Sih. Noordhoff International Publishing, Leyden, 1973.